Contribution from the Department of Molecular Biology, MB1, Research Institute of Scripps Clinic, La Jolla, California 92037

Exchange Coupling and Resonance Delocalization in Reduced $[Fe_4S_4]^+$ and $[Fe_4Se_4]^+$ Clusters. 1. Basic Theory of Spin-State Energies and EPR and Hyperfine Properties

Louis Noodleman

Received April 16, 1990

We develop a theoretical spin-coupling model to describe the energies and properties of the spin eigenstates in reduced $[Fe_4S_4]^+$ and $[Fe_4Se_4]^+$ proteins and their synthetic analogues. Appropriate ranges for the resonance B parameter and the two Heisenberg J parameters can be estimated from our previous quantitative work on related $[ZnFe_3S_4]^+$ systems. This phenomenological model provides a reasonably good account of the EPR and hyperfine properties of typical $S = {}^1/_2$ states of reduced clusters, and we show that it is superior to a Heisenberg model in accounting for these properties and site equivalence patterns. The theory is also successful in describing the coexistence of $S = {}^1/_2$ and ${}^7/_2$ states in reduced Se ferredoxin, including the 3:1 site localization pattern and the corresponding hyperfine properties of the $S = {}^7/_2$ state, as well as the delocalized $S = {}^1/_2$ state. There is a competition between resonance delocalization (governed by the B parameter) and external localizing forces. The $S = {}^7/_2$ state becomes favored over $S = {}^1/_2$ when the ratio between the smaller Fe^{2+}-Fe^{2+} J parameter and the larger Fe^{2+}-Fe^{3+} J parameter is sufficiently small. There is a corresponding spin-state crossing point involving $S = {}^1/_2$, ${}^3/_2$, ${}^5/_2$, and ${}^7/_2$ in parameter space. Properties of $S = {}^3/_2$ states are not well described by the present model; these are more accurately given by the more general model described in a companion paper. Nevertheless, the model outlined here provides a simple phenomenological framework for understanding many features of reduced iron-sulfur and iron-selenium clusters.

I. Introduction

Reduced [4Fe-4S]$^+$ and [4Fe-4Se]$^+$ clusters can have a large variety of spin ground states.[1,2] Among proteins, selenium-substituted reduced clostridial ferredoxin (Cp Fd red),[2] the oxidized P clusters of the MoFe protein of nitrogenase,[3] and the Fe protein (Av2) in *Azotobacter vinelandii* nitrogenase[4] all possess ground states with $S \geq {}^1/_2$, in contrast to the $S = {}^1/_2$ ground state typical of reduced bacterial ferredoxins.[5] Among analogous synthetic $Fe_4S_4(SR)_4^{3-}$ clusters, spin $S = {}^3/_2$ and spin mixtures of $S = {}^1/_2$ and $S = {}^3/_2$ are more common than pure $S = {}^1/_2$ states in the recent studies of Carney et al.[1] The [4Fe-4Se]$^+$ clusters of Se-substituted Cp Fd red are particularly interesting because of the coexistence at low temperatures (even at $T = 1.6$ K) of $S = {}^1/_2$, ${}^3/_2$, and ${}^7/_2$ states.[2] Further, the ratio of equivalent Fe sites is evidently dependent on spin state, with a 2:2 ratio for $S = {}^1/_2$ and a 3:1 ratio for $S = {}^7/_2$. For various bacterial ferredoxins with $S = {}^1/_2$ a similar equivalence of Fe sites in pairs (2:2) is found, while for oxidized P clusters with an $S = {}^7/_2$ or ${}^5/_2$ ground state an approximate 2:1:1 site ratio is observed.[3] For $S = {}^3/_2$ states, Carney et al.[1] have found all four Fe sites to be equivalent in a synthetic [4Fe-4S]$^+$ cluster, while Lindahl et al.[4] have observed a 2:2 site ratio in Av2 on the basis of the hyperfine structure seen with magnetic Mossbauer spectroscopy. In all cases where $S = {}^3/_2$, the hyperfine spectrum is not very well resolved and fitting the data even to simple models is difficult.[1,2,4] The properties of this assortment of states have been extensively studied by a combination of techniques including magnetization and EPR and magnetic Mossbauer[1-6] spectroscopy, but no general model is available that can rationalize the various observations.

In the present work, I will construct a theoretical model to describe the relative energies and properties of the states found in [4Fe-4S]$^+$ clusters. While essentially phenomenological in application, the model is well founded in terms of fundamental theory, and reasonable ranges for the few parameters of the theory can be either estimated from previous quantitative calculations or assessed from regions in parameter space where different spin states coexist or lie close in energy. The requirement that the theory explains both the coexistence of states and their hyperfine and EPR properties acts as a severe constraint on the possible solutions to the problem and as a fairly strong test of viability of the theory itself.

We begin by presenting the results of a simple Heisenberg theory as formulated in the work of G. Papaefthymiou et al.[6] While this theory has some important successes, a detailed analysis demonstrates serious physical problems in the interpretation of site equivalences and EPR and hyperfine properties. By introducing the concept of resonance delocalization and employing Racah algebra, we derive a more general and physically satisfying theory. The full power of theory is only apparent when both hyperfine properties and relative energies are evaluated.

In this paper we develop the basic or linear theory of energies and properties. In the following paper, we present a more general nonlinear theory. The linearity or nonlinearity is with respect to the ratio of Heisenberg parameters for ferrous-ferrous and ferrous-ferric interactions. For both theories, we assume resonance delocalization over one specific pair of mixed-valence sites only, so that there is one B parameter in the problem. Computer codes incorporating the theory developed here may be obtained from the author.

In other iron-sulfur clusters, including [3Fe-4S]^0 and [4Fe-4S]$^{3+,2+}$, resonance delocalization coupling (also called "double exchange") has been recognized as an important determining factor in both the total spin of the system ground state and in the detailed spin-coupling pattern.[8-13] This interaction is also present

(1) Carney, M. J.; Papaefthymiou, G. C.; Spartalian, K.; Frankel, R. B.; Holm, R. H. *J. Am. Chem. Soc.* **1988**, *110*, 6084.
(2) (a) Auric, P.; Gaillard, J.; Meyer, J.; Moulis, J. M. *Biochem. J.* **1987**, *242*, 525. (b) Gaillard, J.; Moulis, J. M.; Auric, P.; Meyer, J. *Biochemistry* **1986**, *25*, 464. (c) Moulis, J. M.; Auric, P.; Gaillard, J.; Meyer, J. *J. Biol. Chem.* **1984**, *259*, 11396.
(3) (a) Huynh, B. H.; Henzl, M. T.; Christner, J. A.; Zimmerman, R.; Orme-Johnson, W. H.; Munck, E. *Biochim. Biophys. Acta* **1980**, *623*, 124. (b) McLean, P. A.; Papaefthymiou, V.; Orme-Johnson, W. H.; Munck, E. *J. Biol. Chem.* **1987**, *262*, 12900. (c) Johnson, M. K.; Thomson, A. J.; Robinson, A. E.; Smith, B. E. *Biochem. Biophys. Acta* **1981**, *671*, 61. (d) Smith, J. P.; Emptage, M. H.; Orme-Johnson, W. H. *J. Biol. Chem.* **1982**, *257*, 2310.
(4) Lindahl, P. A.; Day, E. P.; Kent, T. A.; Orme-Johnson, W. H.; Munck, E. *J. Biol. Chem.* **1985**, *260*, 11160.
(5) Middleton, P.; Dickson, D. P. E.; Johnson, C. E.; Rush, J. D. *Eur. J. Biochem.* **1978**, *88*, 135.
(6) Papaefthymiou, G. C.; Laskowski, E. J.; Frota-Pessoa, S.; Frankel, R. B.; Holm, R. H. *Inorg. Chem.* **1982**, *21*, 1723.
(7) Collision, D.; Mabbs, F. E. *J. Chem. Soc., Dalton Trans.* **1982**, 1573.
(8) Noodleman, L. *Inorg. Chem.* **1988**, *27*, 3677.
(9) (a) Munck, E.; Papaefthymiou, V.; Surerus, K. K.; Girerd, J. J. In *Metals in Proteins*; ACS Symposium Series; Que, L., Ed.; American Chemical Society: Washington, DC, 1988; Chapter 15, pp 302-325. (b) Papaefthymiou, V.; Girerd, J. J.; Moura, I.; Moura, J. J. G.; Munck, E. *J. Am. Chem. Soc.* **1987**, *109*, 4703. (c) Girerd, J. J. *J. Chem. Phys.* **1983**, *79*, 1766. (d) Koppel, H.; Cederbaum, L. S.; Domcke, W.; Shaik, S. S. *Angew. Chem., Int. Ed. Engl.* **1983**, *22*, 210.
(10) (a) Anderson, P. W.; Hasegawa, H. *Phys. Rev.* **1955**, *200*, 675. (b) Borshch, S. A. *Sov. Phys.—Solid State* **1984**, *26*, 1142. (c) Borshch, S. A.; Kotov, I. N.; Bersuker, I. B. *Sov. J. Chem. Phys.* **1985**, *3*, 1009. (d) Borshch, S. A.; Chibotaru, L. F. *Chem. Phys.* **1989**, *135*, 375. (e) Belinskii, M. I. *Mol. Phys.* **1987**, *60*, 793.
(11) Noodleman, L.; Baerends, E. J. *J. Am. Chem. Soc.* **1984**, *106*, 2316.
(12) (a) Noodleman, L.; Norman, J. G., Jr.; Osborne, J. H.; Aizman, A.; Case, D. A. *J. Am. Chem. Soc.* **1985**, *107*, 3418. (b) Aizman, A.; Case, D. A. *J. Am. Chem. Soc.* **1982**, *104*, 3269.

0020-1669/91/1330-0246$02.50/0

Table I. Allowed Values and Range of Spin Quantum Numbers

S	S^* values	S_{12} range
$^1/_2$	2–3	0–4, 1–4
$^3/_2$	1–4	1–3, 0–4, 1–4, 2–4
$^5/_2$	0–5	2, 1–3, 0–4, 1–4, 2–4, 3–4
$^7/_2$	1–6	1–3, 0–4, 1–4, 2–4, 3–4, 4

in reduced $[2Fe–2S]^+$ systems, where it is expected to affect excited states of the spin ladder with large spin S; for the ground spin state of the dimer where $S = {}^1/_2$, the resonance delocalization energy is small and readily overcome by Heisenberg coupling combined with minor asymmetries from the protein or cluster environment.[9,11] Papaefthymiou, Munck, Girerd, and co-workers have presented a clear discussion of the role of double exchange on the energies and properties of $[3Fe–4S]^0$ clusters, including also some comparisons with mixed-valence dimers.[9] Compared to these systems and to the more oxidized forms of 4Fe–4S clusters, reduced $[4Fe–4S]^+$ clusters display more complicated patterns of spin states. These are associated with the low values for the Heisenberg antiferromagnetic coupling constants. Below, we develop the intricate consequences of the interplay of Heisenberg coupling with resonance delocalization in reduced 4Fe–4S clusters.

II. Consequences of a Heisenberg Hamiltonian

We begin by exploring the consequences of a Heisenberg Hamiltonian for the spin states of the reduced clusters $[4Fe–4S]^+$ or $[4Fe–4Se]^+$. Formally, there are three Fe^{2+} sites, which we will designate as sites 1–3, and one Fe^{3+} site called site 4. Each site will have an associated spin vector $\vec{S}_i$ with $i = 1–4$. Then the Heisenberg Hamiltonian for the system is[6,7]

$$H_{Heis} = J_2(\vec{S}_1\cdot\vec{S}_2 + \vec{S}_1\cdot\vec{S}_3 + \vec{S}_2\cdot\vec{S}_3) + J_1((\vec{S}_1 + \vec{S}_2 + \vec{S}_3)\cdot\vec{S}_4) \quad (1)$$

where $J_1 = J(Fe^{3+}–Fe^{2+})$ is the Heisenberg parameter for each mixed-valence pair, $J_2 = J(Fe^{2+}–Fe^{2+})$ is the parameter for each ferrous pair, and $\alpha = J_2/J_1$ is the ratio of these parameters. It turns out that α is a very important variable both for the Heisenberg problem and for the more general problem where resonance delocalization is also considered. (Our convention for the spin vectors will be that for S_i or S_{ij} without the vector sign we are referring to the spin quantum numbers, whereas $\vec{S}_i$ or $\vec{S}_{ij}$ refers to the spin vector itself.) In addition to the spin quantum numbers for the individual sites S_1–S_4, we will need the spin quantum numbers for three Fe^{2+} sites coupled together $S^* = S_{123}$, for the first two of these sites S_{12}, and for the total system spin S.

For the Heisenberg Hamiltonian written in eq 1, the problem is readily solved in closed form to given the energy eigenvalues $E(S,S^*)$

$$E(S,S^*)/J_1 = (\alpha - 1)S^*(S^* + 1)/2 + S(S + 1)/2 \quad (2)$$

We write the eigenstates as $|S\ S^*\ S_{12}\rangle$, sorting and classifying these according the triangle inequality.[8–10] For given S and S_4 values where $S_4 = {}^5/_2$ and $S_1 = S_2 = S_3 = 2$, the triangle inequality gives

$$\begin{gathered} |S + S_4| \geq S^* \geq |S - S_4| \\ S_{max}{}^* \leq 6 = |S_1| + |S_2| + |S_3| \end{gathered} \quad (3)$$

$$|S^* + S_3| \geq S_{12} \geq |S^* - S_3| \qquad S_{12} \leq 4 = |S_1| + |S_2| \quad (4)$$

The ranges of the spin quantum numbers for different possible values of the total system spin are summarized in Table I.

Two consequences of the Heisenberg Hamiltonian are immediately apparent: first, for $\alpha < 1$ the lowest energy states for each total S value have S^* maximal (see eq 2); second, the spin states are degenerate in S_{12}. The range $\alpha < 1$ is expected, since both experimental and theoretical studies on Fe–S clusters have found

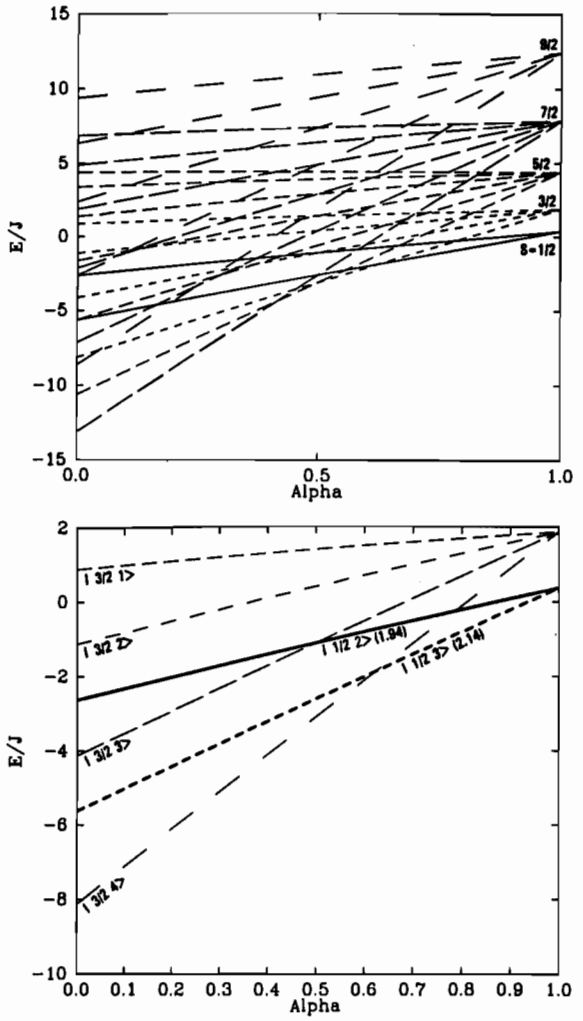

Figure 1. (a) Top: Heisenberg Hamiltonian energies plotted versus α for total S from $^1/_2$ to $^9/_2$. (b) Bottom: Heisenberg Hamiltonian energies and states specified by quantum numbers $|S\ S^*\rangle$ for $S = {}^1/_2$ and $^3/_2$. Calculated g_{av} values for the $S = {}^1/_2$ states are given in parentheses. The energy scale is expanded compared to (a).

$J(Fe^{3+}–Fe^{2+}) > J(Fe^{2+}–Fe^{2+})$. Parts a and b of Figure 1 show the predicted energy eigenstates of the Heisenberg Hamiltonian eq 2 in the range $0 \leq \alpha \leq 1$. Figure 1b gives the energy eigenstates for $S = {}^1/_2$ and $^3/_2$ on an expanded scale E/J_1. The eigenvectors are specified by $|S\ S^*\rangle$. Each line represents several degenerate states, since there is a range of values of S_{12} for fixed S and S^* (see Table I). In Figure 1a, states having total $S = {}^1/_2$, $^3/_2$, $^5/_2$, and $^7/_2$ become the lowest successively as α decreases from 1 to 0. States with $S = {}^9/_2$ are never lowest, since $S_{max}{}^* \leq 6$ and, by eq 2, there will always be an $S = {}^7/_2$ state below any $S = {}^9/_2$ state. In Figure 1b, we can see that the state $|S\ S^*\rangle = |{}^1/_2\ 3\rangle$ lies below $|{}^1/_2\ 2\rangle$ and that $|{}^3/_2\ 4\rangle$ is lower than $|{}^3/_2\ 3\rangle$, $|{}^3/_2\ 2\rangle$, or $|{}^3/_2\ 1\rangle$. The crossing point from $|{}^1/_2\ 3\rangle$ to $|{}^3/_2\ 4\rangle$ occurs at $\alpha = 0.63$. At $\alpha = 1$ we recover a Heisenberg Hamiltonian with all J parameters equal and energy levels that depend solely on total S as $E(S) = J_1S(S + 1)/2$. Papaefthymiou et al.[6] have solved a similar Hamiltonian including also the isotropic Zeeman term for selected values of J_1 and J_2. Our results are completely consistent with their Figure 5 in terms of energies and degeneracies; in addition, Figure 1 and Table I show how the energy states change with $\alpha = J_2/J_1$ and specify the spin states in more detail. (A diagram analogous to Figure 1a may be found in Collision and Mabbs,[7] but it is erroneous; for example, the crossing points at $\alpha = 1$ are absent. These crossing points follow directly from the degeneracies at $\alpha = 1$ shown by eqs 2–4.)

The various spin-state crossings in Figure 1 are suggestive of the behavior observed in some reduced $[Fe_4S_4]^+$ clusters where coexisting $S = {}^1/_2$, $^3/_2$, and/or $^7/_2$ states are found. However,

(13) (a) Noodleman, L.; Case, D. A.; Sontum, S. F. *J. Chim. Phys.* **1989**, *86*, 743. (b) Sontum, S. F.; Noodleman, L.; Case, D. A. In *The Challenge of d and f Electrons Theory and Computation*; ACS Symposium Series 394; Salahub, D. R., Zerner, M. C., Eds.; American Chemical Society: Washington, DC, 1989; Chapter 26, pp 366–377.

a closer examination of the properties of the lowest lying eigenstates of the Heisenberg Hamiltonian shows that a more complicated spin Hamiltonian is needed to describe such phenomena reasonably. Specifically, the Heisenberg model exhibits the following problems: First, because there are three Fe^{2+} sites and a unique Fe^{3+} site, we would expect a 3:1 pattern of equivalent sites for A values and for Mossbauer properties like ΔE_Q and δ. By contrast, for the $S = {}^1/_2$ states of $[Fe_4S_4]^+$ clusters, the sites are typically equivalent in pairs (2:2 pattern) as indicated by Mossbauer A values and isomer shifts δ.[1,2] These results are consistent with the presence of a specific resonance-delocalized pair of oxidation state $Fe^{2.5+}$–$Fe^{2.5+}$ and of a separate ferrous pair (Fe^{2+}–Fe^{2+}). Second, for the Heisenberg model, the lowest energy $S = {}^1/_2$ state for $\alpha < 1$ is $|S\,S^*\rangle = |{}^1/_2\,3\rangle$, which has a predicted value of $g_{av} = 2.14$ (approximately) in contrast to typical experimental values in the range $g_{av} = 1.94$–1.96. Further the mixed-valence Fe^{2+}–Fe^{3+} (equivalently $2Fe^{2.5+}$) pair is calculated to have a positive A value, while experimentally this A value is about −30 MHz. The calculated A value for the ferrous pair also has the wrong sign compared to experiment. (The theoretical methods for calculating approximate g and A values for a specified spin state will be explained in detail in section VI.) In contrast to this, a state having a specific delocalized pair with $|S\,S^*\,S_{12}\rangle = |{}^1/_2\,2\,4\rangle$ exhibits a predicted $g_{av} = 1.94$, mixed-valence pair A value of −33 MHz, near the experimental values −30 to −34 MHz, and a ferrous pair predicted A value of +24.4 MHz compared to 15–16 MHz experimental. The level of agreement of this delocalized state with experiment suggests that for $S = {}^1/_2$ a state with $S^* = 2$ lies below $S^* = 3$. This is not possible in the context of a Heisenberg Hamiltonian alone, but it is the predicted behavior when resonance over a mixed-valence pair is taken into account. This provides a practical motivation for the theoretical developments in the next section.

III. Effects of Resonance Delocalization and of Localizing Forces

For a mixed-valence pair of metal sites where the individual metal ions have net spin as in high-spin Fe^{2+} interacting with high-spin Fe^{3+}, the electron delocalization energy depends on the degree of parallel alignment of the site spins. In fact, this energy is linear in the pair spin quantum number S_{34}.[8-13] This idea appears in the early work of Anderson and Hasegawa.[10a] It has been developed or rediscovered by several research groups, including our own,[8-13] and there are two distinct mathematical proofs that this term is proportional to $(S_{34} + {}^1/_2)$.[10a-11] Where there is significant metal–metal orbital overlap (or ligand-mediated metal–metal overlap), there is then an important term that must be added to the Heisenberg Hamiltonian. This term is called "resonance delocalization", "double exchange", or simply the "B term".[8-13] $10B$ is essentially twice the hopping integral for the site orbitals that contain the extra electron of the mixed-valence pair.[13]

Defining the sites and the spin vectors as in the preceding section, we introduce a resonance interaction between sites 3 and 4 so that the total Hamiltonian is[8,9]

$$H_{tot} = H_{Heis} + H_{reson} = H_{Heis} - BT_{34} \qquad (5)$$

where B is the resonance delocalization parameter and T is the transfer operator for the subdimer with sites 3 and 4. The effect of the operator T_{34} is to generate the factor $S_{34} + {}^1/_2$ under the condition that the subdimer spin quantum number S_{34} is a good quantum number when applied to the appropriate spin-state function. This is achieved by expressing each spin-state function as a linear combination of states with pure S_{34} quantum numbers; that is, by expressing each spin state (ket) in the appropriate representation. It is necessary to define two spin kets $|A\rangle$ and $|B\rangle$ as

$$|A\rangle = |(S_{12}S_3{}^A)S_A{}^*S_4{}^AS\rangle^A = \sum_{S_{34}} U(S\,S_{34}\,S_A{}^*S_{12})|(S_{12})(S_{34}{}^A)S\rangle \qquad (6)$$

$$|B\rangle = |(S_{12}S_4{}^B)S_B{}^*S_3{}^BS\rangle^B = \sum_{S_{34}} U(S\,S_{34}\,S_B{}^*S_{12})|(S_{12})(S_{34}{}^B)S\rangle$$

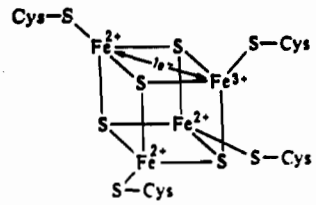

Figure 2. Structure and valence delocalization diagram for $[Fe_4S_4(SR)_4]^{3-}$. Sites 1 and 2 are the two Fe^{2+}'s at the bottom of the diagram. The resonance pair are sites 3 and 4, Fe^{2+}–Fe^{3+} depicted at the top.

where $S_A{}^* = S_{123}{}^A$ and $S_B{}^* = S_{124}{}^B$. The first two spin vectors specified (in parentheses) are coupled to $S_A{}^*$ or $S_B{}^*$, respectively, and this is coupled to the final site vector $S_4{}^A$ or $S_3{}^B$ to give S. The right-hand side of eq 6 gives an alternative coupling scheme where S_3 and S_4 are coupled together to give S_{34} before being combined with S_{12}. The sets of vectors on the left- and right-hand sides of the equation span the same vector space and are related by a unitary transformation given by the unitary matrix U. These coefficients are closely related to Racah coefficients and to Wigner $6j$ symbols.[14] Essentially, states where S^* and S are good quantum numbers are expressed as linear combinations of states where S_{12}, S_{34}, and S are good quantum numbers.

The state $|A\rangle$ has the unique Fe^{3+} center on site 4 so that $S_4 = {}^5/_2$ and the three Fe^{2+} sites have $S_1 = S_2 = S_3 = 2$, whereas for state $|B\rangle$ one electron has shifted from site 3 to site 4 so that $S_3 = {}^5/_2$ and $S_1 = S_2 = S_4 = 2$. The Fe^{3+} site is then site 3. (Figure 2 shows the structure and the Fe valences.) Both spin states of type $|A\rangle$ and of type $|B\rangle$ are localized eigenstates of a Heisenberg Hamiltonian H_{Heis} acting alone. When considering the electron-transfer resonance, it is necessary that the J values J_1 and J_2 for the spin coupling between pairs of sites be permuted to correspond to the valence of the site for these two possible localized states. Formally this is achieved by permuting the indices 3 and 4 of $\bar{S}_3$ and $\bar{S}_4$ in eq 1 when H_{Heis} is applied to states $|B\rangle$ in place of states $|A\rangle$. The solutions to the eigenvalue problem are still given by eq 2 with $S^* = S_A{}^*$ for $|A\rangle$ and $S^* = S_B{}^*$ for $|B\rangle$. Further, states $|A\rangle$ and $|B\rangle$ form basis states for the solution of H_{tot} (eq 5). The effect of the transfer operator is defined by

$$BT_{34}|(S_{12})(S_{34}{}^A)S\rangle = B(S_{34} + {}^1/_2)|(S_{12})(S_{34}{}^B)S\rangle \qquad (7)$$

The parameter B is proportional to a transfer or hopping integral of the interacting d orbitals on sites 3 and 4.[8-13] The magnitude of B will depend upon the precise spatial character of the two interacting Fe 3d orbitals on adjacent sites and will be linked to the overall electronic structure of the cluster. This, in turn, is a function of the covalently bonded ligand structure of bridging S and especially terminal SR groups, as well as of detailed cluster geometry, solvent environment, possible hydrogen bonding, counterions, and other effects of the protein or cluster environment.[11-13]

To determine the important resonance effects in the simplest manner, we will consider initially only the degenerate mixing of state $|A(S)\rangle$ with $|B(S)\rangle$. The resonance matrix elements are

$$-E_{res} = \langle B(S)|H_{res}|A(S)\rangle = -\sum_{S_{34}} B(S_{34} + {}^1/_2)[U(S\,S_{34}\,S_A{}^*S_{12})]^2 \qquad (8a)$$

with the bounds on S_{34} determined by

$$|S + S_{12}| \geq S_{34} \geq |S - S_{12}| \qquad (8b)$$

and

$$S_{34} \leq S_3 + S_4$$

(14) (a) Brink, D. M.; Satchler, G. R. *Angular Momentum*, 2nd ed.; Oxford University Press: London, 1968. (b) Edmonds, A. R. *Angular Momentum in Quantum Mechanics*; Princeton University Press: Princeton, NJ, 1957; Chapter 6, pp 90–108. (c) Wigner, E. P. *Group Theory*; Academic Press: New York, 1959; Chapter 27, pp 349–356. (d) Griffith, J. S. *Struct. Bonding (Berlin)* **1972**, *10*, 87. (e) Munck, E. *Meth. Enzymol.* **1978**, *54*, 346.

Further

$$[U(S\ S_{34}\ S_A{}^*S_{12})]^2 = (2S_A{}^* + 1)(2S_{34} + 1)\begin{Bmatrix} S & S_{12} & S_{34}{}^A \\ S_3{}^A & S_4{}^A & S_A{}^* \end{Bmatrix}^2 \quad (9)$$

where $\{\}$ is a Wigner $6j$ symbol.[14] Defining also E_{Heis} as the energy $E(S,S^*)$ in eq 2, we can then formulate an energy eigenvalue equation including both Heisenberg and resonance interactions:

$$\begin{bmatrix} E_{Heis} - E & -E_{res} \\ -E_{res} & E_{Heis} - E \end{bmatrix}\begin{bmatrix} c_A \\ c_B \end{bmatrix} = 0 \quad (10)$$

There may also be a site inequivalence due to external forces. If we allow the local states $|A\rangle$ and $|B\rangle$ to be shifted by an external localizing energy $\pm E_{loc}/2$, then the eigenvalue equation becomes

$$\begin{bmatrix} E_{Heis} - E_{loc}/2 - E & -E_{res} \\ -E_{res} & E_{Heis} + E_{loc}/2 - E \end{bmatrix}\begin{bmatrix} c_A \\ c_B \end{bmatrix} = 0 \quad (11)$$

Scaling the localizing energy by B, we let $f_{loc} = E_{loc}/B$. It is also useful to define a scaled resonance energy by $f_{res} = E_{res}/B$, since by eq 8 and 9 this will be determined by the coupled spin states alone and is, in fact, $\langle S_{34} + {}^1/_2\rangle$ for each such state $|A(S)\rangle$ or $|B(S)\rangle$.

The quantity $-E_{loc}/2$ represents the site stabilization energy. In a vibronic coupling model, this is the stabilization energy due to the coupling of the extra electron's energy to an odd normal mode displacement $\lambda Q_u = E_{loc}/2$, where the product of the displacement Q_u and electron-vibration coupling parameter λ acts to localize the extra electron of the mixed-valence pair to a particular site.[9c,d] More generally, localization can also derive from the protein electrostatic environment, from solvent coordination, or from hydrogen bonding. For example, the protein may act as a dipolar field on the cluster, or the interaction may be more complex. We estimate the magnitude for this localization energy necessary to account for the delocalized $S = {}^1/_2$, localized $S = {}^7/_2$ coexistence in section VI. The detailed origin of the localizing forces on reduced 4Fe-4Se proteins is an important open question.[2]

Returning to the mathematical formulation of the problem, in the presence of resonance delocalization and with no external localizing forces (eq 10), we find $c_A = 2^{-1/2}$ and $c_B = \pm 2^{-1/2}$. In the presence of a localizing force $0 \le |c_A|, |c_B| \le 1$, and $c_A{}^2 + c_B{}^2 = 1$. In general, there is partial localization that becomes large when $E_{loc}/2 \gg E_{res}$. We will demonstrate later than this behavior rationalizes the crossover of a localized $S = {}^7/_2$ state and a related but delocalized $S = {}^1/_2$ state so that both states may be simultaneously present as in certain Se-substituted reduced ferredoxins.

Important general consequences of this model are as follows: (1) E_{res} splits states by lifting the degeneracy of the states in S_{12} (see Table I) from $|S\ S^*\rangle$ to $|S\ S^*\ S_{12}\rangle$ with energy

$$E(S,S^*,S_{12})_\pm = E_{Heis} \bullet E_{res} \quad (12)$$

(2) E_{res} and E_{loc} together produce partly localized states with energies

$$E(S,S^*,S_{12})_{1,2} = E_{Heis} + (E_{RL})_{1,2} \quad (13)$$

The eigenvalues and eigenvectors can be determined from simplified equations (by noticing that E_{Heis} acts as a constant along the diagonal of the matrices in eqs 10 and 11):

$$\begin{bmatrix} -E_{loc}/2 - E_{RL} & -E_{res} \\ -E_{res} & +E_{loc}/2 - E_{RL} \end{bmatrix}\begin{bmatrix} c_A \\ c_B \end{bmatrix}_{1,2} = 0 \quad (14)$$

$$(E_{RL})_{1,2} = \pm[E_{loc}{}^2/4 + E_{res}{}^2]^{1/2} = \pm B[f_{loc}{}^2/4 + f_{res}{}^2]^{1/2} \quad (15)$$

After solving eqs 12–14 by standard methods, we can assess state crossings and obtain state energies and properties as a function of the B and J_1 and J_2 parameters.

A few comments on our choice of phase are appropriate. The sign of $-E_{res}$ in eqs 8 and 10 and of the resonance Hamiltonian in eq 5 are chosen so that positive B gives the lowest energy (minus root in eq 15) for the positive bonding combination of c_A and c_B. This is the expected situation for the lowest electronic state. This is the same convention assumed in our phenomenological treatment of high-potential clusters;[8] our recent quantitative calculations on FeS clusters report B using the opposite convention for the off-diagonal matrix elements so that B is negative.[13] Table III reports resonance interaction parameters with the convention of positive B. The sign convention is always well defined when the resonance Hamiltonian or the corresponding resonance matrix are specified explicitly. Further, for the $[Fe_4S_4]$ cluster problem, the energy eigenvalues are independent of the sign convention for B.

I have written a set of computer codes to implement the appropriate algorithms. The Racah coefficient subroutine used was written by J. P. Desclaux, and the matrix diagonalization subroutine was written by D. F. Mayers and J. P. Desclaux utilizing the QR method. The matrix diagonalization routine was also used for the larger matrices found in the companion paper. Calculations were performed on a Convex C1 computer at Scripps, and plotting utilized a SUN 3/50 computer.

In the next section, we consider orbital aspects of the resonance delocalization interaction.

IV. Orbitals and Electron Delocalization

For the methods developed above to be useful in practice, it is necessary to have some idea of what regions in parameter space correspond to the electronic structure of the reduced 4Fe ferredoxins, as well as whether the number and type of parameters assumed are really adequate for the physical situation. While we have not as yet completed quantitative calculations of J and B parameters for reduced $[Fe_4S_4(SR)_4]^{3-}$ clusters by density functional methods, we do have corresponding results for doubly reduced $[ZnFe_3S_4(SR)_4]^{3-}$, where the Fe atom oxidation levels are equivalent;[13] essentially, one localized Fe^{2+} site is replaced by a Zn^{2+}. The three iron centers of the $ZnFe_3$ cluster consist of a trapped-valence Fe^{2+} site and a delocalized mixed-valence pair $2Fe^{2.5+}$. Both our calculations and experimental Mössbauer data on reduced Fe_4S_4 clusters having $S = {}^1/_2$ give a general picture analogous to the $[ZnFe_3S_4]^+$ cluster.

Our previous calculations on $[ZnFe_3S_4]^+$ as well as on $[Fe_4S_4]^{3+,2+,+}$ and $[Fe_3S_4]^0$ showed that the electronic ground state had a high-lying Fe–Fe σ-bonding orbital containing $1e^-$ (of minority spin) extending over the mixed-valence Fe^{3+}–Fe^{2+} pair.[12,13] Further, this orbital is largely confined to one $Fe_2S_2(SR)_2$ layer of the iron–sulfur cubane structure, and is directed across one face diagonal of the cube. For $[ZnFe_3S_4]^{2+}$, $[Fe_3S_4]^0$, and $[Fe_4S_4]^{3+}$ there is one such orbital occupied;[13] for $[Fe_4S_4]^{2+}$, there are two such orbitals on opposite faces of the cube, $20a_1\alpha$ and $20a_1\beta$ in the broken symmetry C_{2v}.[12] (The idealized geometry of the cluster is D_{2d}.) For $[Fe_4S_4]^+$, three high-lying Fe orbitals are involved.[12] Two of these resemble the corresponding orbitals of the 2+ cluster, while the third may be either an Fe–Fe σ^*-antibonding orbital or an Fe–Fe δ^*-antibonding orbital. These alternative levels $9a_2\alpha$ and $14b_2\alpha$ are nearly degenerate in energy, within 0.12 eV. The delocalized electron within the mixed-valence pair is associated with the single Fe–Fe σ-bonding orbital $20a_1\beta$. The orbitals $20a_1\alpha$ and $9a_2\alpha$ (or alternatively $14b_2\alpha$) are associated with the ferrous pair.

The orbital level diagram of $[Fe_4S_4]^+$ is shown in Figure 3 taken from our previous work using density functional methods.[12] We can denote the two relevant orbital configurations as OC1 = $(20a_1\alpha\ 20a_1\beta\ 14b_2\alpha)$ and OC2 = $(20a_1\alpha\ 20a_1\beta\ 9a_2\alpha)$, with a_1 as σ, b_2 as σ^*, and a_2 as δ^*. The spin indices α and β are also associated with the spatial distribution of the orbitals, which are largely confined to the opposite faces of the cube (bottom and top, respectively) in the broken C_{2v} symmetry of the cluster. With the conventions above, for orbital filling the $2Fe^{2+}$ pair is at the bottom of the cube and the mixed-valence Fe^{3+}–Fe^{2+} pair lies at the top, as shown in Figure 2. Table II compares the results of our previous calculations of isomer shifts δ and Mossbauer quadrupole splittings ΔE_Q for OC1 and OC2 with those in a

Table II. Mössbauer Quadrupole Splittings and Isomer Shifts for $[Fe_4S_4]^+$ and $[Fe_4S_4]^+$

spin	cluster	ΔE_Q[a] oxid	ΔE_Q[a] red	δ[a] oxid	δ[a] red	ref
			Theory			
	$20a_1^2 9a_2$ (OC2)	1.36	1.43	0.57	0.62	12a
	$20a_1^2 14b_2$ (OCl)	1.41	−2.63			
			Experiment			
$^1/_2$	Av2/ethylene glycol	0.98	1.60	0.53	0.59	4
	Cp Fd	1.05	1.70	0.50	0.55	2a
	Cp Se Fd	1.14	1.50	0.48	0.53	2a
	syn **1** (Carney)	0.94	2.07	0.40	0.48	1
	B. stearo Fd	1.32	1.89	0.50	0.58	5
$^3/_2$	Av2/urea	0.8	1.2	0.54	0.54	4
	Cp Se Fd	1.0		0.56		2a
	syn **2** (Carney)	0.96		0.44		1
$^5/_2$	$2P_{ox}$	0.57	−0.72, 1.26	0.40	0.49, 0.48	3a
		0.60	−1.40, +1.53	0.25	0.56, 0.64	
			+3.20, +2.30		0.65, 0.68	
$^7/_2$	Cp Se Fd	1.17	1.67	0.39	0.67	2a

[a] Units: mm/s.

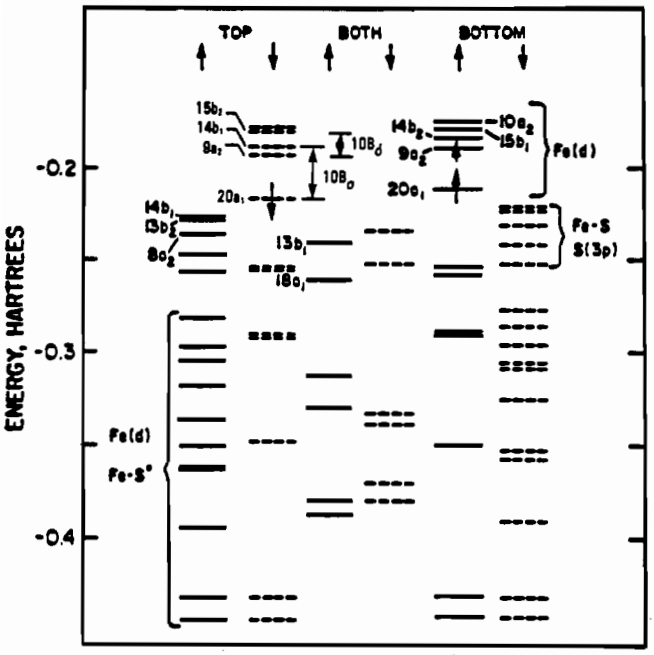

Figure 3. Orbital energy diagram for $[Fe_4S_4(SR)_4]^{3-}$ with R = CH_3 from ref 12a. The lowest energy configuration OC2 is depicted with arrows.

variety of $[Fe_4S_4]^+$ clusters.[12] For the ferrous pair the predicted electronic distribution is highly directional for OC1 and less so for OC2; the idealized electron configuration for these sites is $(d^5\beta\, d_\sigma{}^1\alpha)$–$(d^5\beta\, d_\sigma{}^1\alpha)$ in OC1 and $(d^5\beta\, d_\sigma{}^{1/2}\, d_\delta{}^{1/2}\alpha)$–$(d^5\beta\, d_\sigma{}^{1/2}\, d_\delta{}^{1/2}\alpha)$ in OC2. We have included here the lower lying majority spin Fe 3d levels to obtain a proper d-electron count.[12,15] Corresponding to this, in Table II the predicted ferrous sites' ΔE_Q are larger for OC1 than for OC2. Since these two configurations are very close in energy, we can expect considerable variability in the ferrous sites' ΔE_Q when comparing different proteins and synthetic analogues. For the mixed-valence pair, the predicted difference in ΔE_Q is much smaller, since for both OC1 and OC2, the electronic asymmetry is induced by the same orbital $20a_1\beta$. (The self-consistent fields and the corresponding orbitals differ in only minor ways on the mixed-valence pair comparing OC1 and OC2.) Further, the theoretical ferrous pair ΔE_Q is consistently larger in magnitude than that of the mixed-valence pair (designated as red and ox sites, respectively), and so is the isomer shift δ as expected. These theoretical results are in good correspondence with the experimental observations. The ferrous sites' ΔE_Q are consistently larger than the corresponding mixed-valence pair ΔE_Q's and display more variability from cluster to cluster. The isomer shifts order as expected within a given cluster. The only significant exceptions are the $S = {}^3/_2$ clusters where all isomer shifts are indistinguishable to within experimental resolution.

In many of the clusters, sites are roughly equivalent in pairs. The major exceptions are the clear 3:1 site ratio exhibited by the $S = {}^7/_2$ state in Cp Se Fd, the equivalence or near equivalence of sites in $S = {}^3/_2$ clusters (Av2 in urea displays pairwise equivalence; other clusters display complete equivalence of sites), and the very low site equivalence exhibited by oxidized P clusters (all sites are inequivalent with a very approximate 2:1:1 site ratio for $2Fe^{2+}$–Fe^{2+}–Fe^{3+} on the basis of Mössbauer isomer shifts, quadrupole splittings, and hyperfine spectra).

It is helpful also to think about the idealized Fe 3d occupancies and the implications of these for the directionality, strength, and number of B parameters in the problem. For the Fe^{2+}–Fe^{2+} pair, there is a d^6–d^6 interaction, while for the mixed-valence Fe^{3+}–Fe^{2+} pair there is a resonating d^6–d^5 interaction. If the electron delocalization is confined within a layer, a single B parameter is required only for the mixed-valence pair. If, however, the sixth d electron of either site in the ferrous layer can interact strongly with the ferric site in the other layer, then more than one B parameter will be required. In this case, the spin algebra of the problem will be considerably more complicated, there will be more relevant B parameters, and there are more difficulties in exploring parameter space. The results in this paper and the following companion paper are consistent with the idea that the most important features of the hyperfine A and EPR g values are determined by resonance over a single mixed-valence pair. There may be subsidiary resonances between layers; this is currently under investigation by our group and by V. Papaefthymiou, Girerd, and Munck.[16] Such resonances would typically involve σ^* and δ^* orbitals from one layer interacting with the corresponding σ^* or δ^* of the adjacent layer. The important energy terms for interlayer resonance are of the form $-B'\langle S_{ik} + {}^1/_2\rangle$, where i = 1 and 2 and k = 3 and 4. (S_{ik} always refers to a mixed-valence pair and so has half-integer spin.) For most of the low-lying spin states, $\langle S_{ik} + {}^1/_2\rangle$ is expected to be smaller than $\langle S_{34} + {}^1/_2\rangle$, since both S_{34} and S_{12} are large and S is small (particularly for $S = {}^1/_2$ and ${}^3/_2$). The other relevant factor is, of course, B'. Due to the reduced spatial overlap, we would expect the B' parameter governing such interactions to be considerably smaller than the main B parameter of the mixed-valence pair; we are currently

(15) As a consequence of covalent bonding and the associated charge transfer from the sulfur ligands, the actual d-electron count is higher on all Fe's than the idealized "atomic valence state" values given in the text. This is discussed in detail in ref 12.

(16) Papaefthymiou, V.; Girerd, J. J.; Munck, E. Personal communication.

Table III. Spin Hamiltonian Parameters (cm^{-1})

compd	J_{ox}	J_{red}	B'	B	J_{red}/J_{ox}	$\lvert B/J_{red}\rvert$
$Fe_2S_2^{2+/+}$	530	346		+516	0.65	1.5
$Fe_3S_4^{+/0}$ linear	544[a]	407[a]		+568	0.75	1.4
$Fe_3S_4^{+/0}$ cubane	369	297	+30	+406	0.81	1.4
$ZnFe_3S_4^{3+/2+}$	360	282	+28	+407	0.78	1.4
$ZnFe_3S_4^{+}$		45[b]	+64	+426	0.16[c]	9.5
$Fe_4S_4^{3+/2+}$ cube C_{2v}	416	401	+212	+585	1.04	1.5
$Fe_4S_4^{3+}$ sym C_{2v}	416		+216	+561		1.3 (ox)
$Fe_4S_4^{3+}$ sym C_2	359		+103	+605		1.7 (ox)

[a] J value for neighboring irons; J values connecting the two "outside" iron atoms are very small; see ref 13. [b] From eqs 7 and 8 of ref 13a; if the more general more (eqs 9 and 10) is used, then B and B' are unchanged, and $J = 66\ cm^{-1}$ and $\Delta J = -80\ cm^{-1}$. [c] Ratio for the +1 and +2 oxidation states.

working on quantitative calculation of the B' parameter for reduced clusters. The expected magnitude for the interlayer versus intralayer (mixed-valence pair) resonance in $[Fe_4S_4]^+$ should resemble the corresponding B'/B ratio for Fe_3S_4 and $ZnFe_3S_4$ clusters given in Table III, about $^1/_6$.[13] (In the latter case, B' is the parameter governing symmetric delocalization over all Fe sites for parallel alignment of all spin vectors, while B is the interaction parameter for the mixed-valence pair; there is parallel spin alignment within this pair and opposite alignment to the third spin site in the ground state.) Very recently, we have also obtained B'/B ratios for the $[Fe_4S_4]^{3+,2+}$ cluster oxidation states in C_{2v} and C_2 symmetries.[17] These ratios vary between about $^2/_5$ and $^1/_6$ and indicate the general order of magnitude expected for the B'/B ratio in reduced $[Fe_4S_4]^+$ clusters.

Table III summarizes the current status of our calculations of B and J parameters for Fe–S clusters.[11-13,17] It is particularly worth noting that the large B values calculated all refer to a σ-type delocalization over a specific pair with parameter B_σ. Our calculations[12,17] on electronic excited states of Fe_4S_4 clusters show that as expected from considerations of orbital overlap[11] $|B_\sigma| \geq |B_\pi| > |B_\delta|$ (within a layer). Also highly significant is the small value of J and negative ΔJ value given for $ZnFe_3S_4^+$, where, in our notation, $J_1 = J$ and $J_2 = J + \Delta J$ (see footnote b in the caption to Table III). The calculated values of the parameters are $J_1 = 66\ cm^{-1}$, $J_2 = -14\ cm^{-1}$, and $B = 426\ cm^{-1}$. J_1 is antiferromagnetic (AF) and J_2 is ferromagnetic (F). These values should be indicative of the general range of values expected for reduced $[Fe_4S_4]^+$ clusters. There will be considerable variability in parameters due to geometric and environmental perturbations, as cited previously. Further, each electronic orbital state (electronic configuration) will have its own optimal J and B parameters. As an example of the effects of asymmetry, lowering of the effective symmetry below C_{2v} by a geometric or electrostatic perturbation could give σ–δ^* or σ–π^* mixing leading to a "bent Fe–Fe bond" on the mixed-valence pair with an associated lowering of the B value. Overall, our calculated results broadly support models like that explored here, having a single B and two J parameters.

V. Relative Spin-State Energies

From the ideas developed in the previous section, we can construct reasonable ranges for exploring parameter space. (See ref 6 for the "Heisenberg model" experimental J values.) Roughly, we expect $40\ cm^{-1} \leq J_1 \leq 120\ cm^{-1}$; corresponding to this, we have searched parameter space for $-0.5 \leq \alpha \leq 1$ and $0 \leq B/J_1 \leq 6$. From the parameters calculated above, typical ratios should be $B/J_1 = 6$ and $\alpha = -0.2$. Since $|B_\sigma/B_\delta| \geq 2$, a highly bent Fe–Fe bond should be associated with $B/J_1 \leq 3$ approximately. (This $|B_\sigma/B_\delta|$ ratio arises from level separations between various high-lying levels of mainly Fe 3d character (β spin top) as depicted in Figure 3 based on ref 12a. The appropriate ratio is about $|B_\sigma/B_\delta| = 2.0$.) We have made an extensive set of computer calculations for B and α in the range above and present important representative results. Figure 4a illustrates the lowest lying states for each total spin S at $B/J_1 = 6$ in the presence of resonance stabilization but with no localizing force. Over the α range from −0.5 to 1.0, $|S\ S^*\ S_{12}\rangle = |^1/_2\ 2\ 4\rangle$ is the lowest state, lying substantially below $|^1/_2\ 3\ 4\rangle$. A region of rapid state crossings is found near $\alpha = -0.5$. At α values below this $|^7/_2\ 6\ 4\rangle$ becomes the lowest state. Notice that the nature of the spin Hamiltonian allows us to compare the energies of states at the same point in parameter space but not to compare states at different points in parameter space. This is because the electronic and geometric

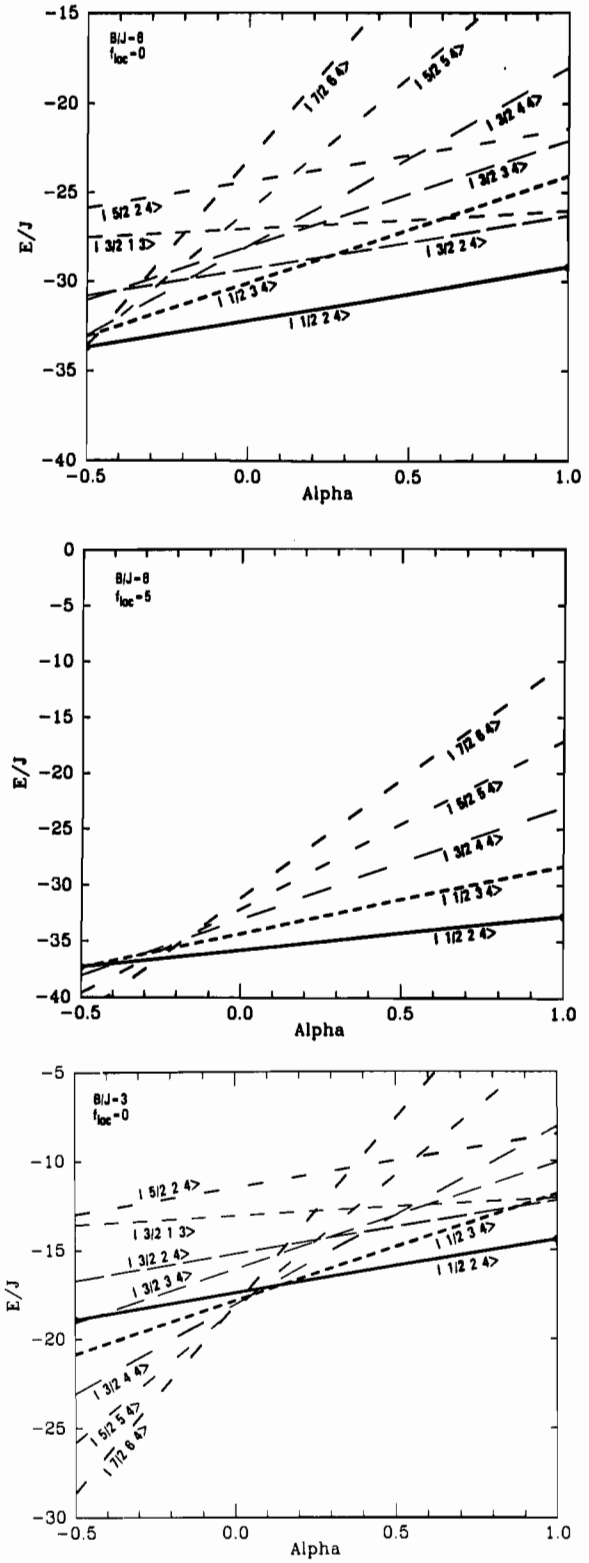

Figure 4. (a) Top: Energies of the low-lying spin states $|S\ S^*\ S_{12}\rangle$ shown at $B/J = 6$ and $f_{loc} = 0$ having delocalization over two sites. (b) Middle: Lowest energy state of each spin plotted with partial localization $f_{loc} = 5$ and $B/J = 6$. (c) Bottom: Energies of the low-lying spin states at $B/J = 3$ and $f_{loc} = 0$.

(17) Noodleman, L.; Case, D. A. Unpublished work.

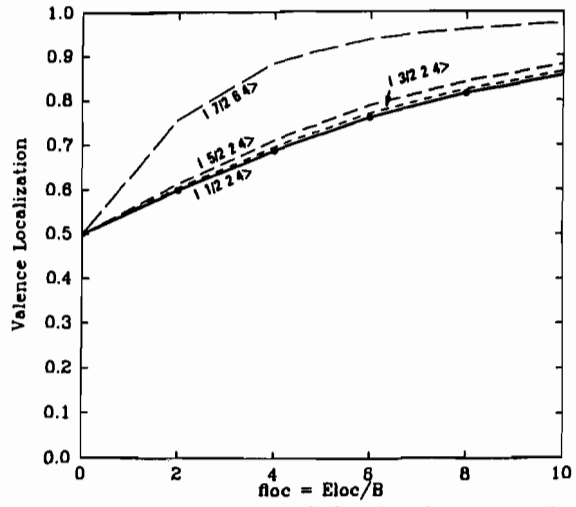

Figure 5. Valence localization versus f_{loc} for selected states. Localization is greatest for $|^7/_2\ 6\ 4\rangle$ and successively less for $|^5/_2\ 2\ 4\rangle$, $|^3/_2\ 2\ 4\rangle$, and $|^1/_2\ 2\ 4\rangle$.

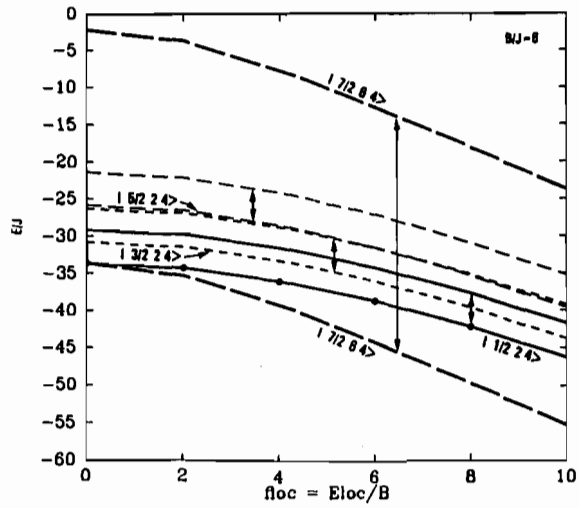

Figure 6. Upper and lower energy bounds are depicted for four states $|S\ S^*\ S_{12}\rangle = |^1/_2\ 2\ 4\rangle$, $|^3/_2\ 2\ 4\rangle$, $|^5/_2\ 2\ 4\rangle$, and $|^7/_2\ 6\ 4\rangle$ at $B/J = 6$ and $-0.5 \le \alpha \le 1$.

dependence of the state energies do not appear directly in the spin Hamiltonian; rather the optimization of these plays a critical role in determining energetically optimal B and J_1 and J_2 parameters. With no localizing force, all states are pairwise delocalized due to the B term.

For Se-substituted reduced Cp Fd, we recall the coexistence of an $S = {}^1/_2$ state with equivalence in pairs, an $S = {}^3/_2$ state with a single broad signal (so that there may be some inequivalence among sites which remains unresolved), and an $S = {}^7/_2$ state with equivalent sites in the ratio 1:3, representing the antiferromagnetic coupling of a single localized Fe^{3+} site with $S_4 = {}^5/_2$ to three Fe^{2+} sites having total spin $S^* = S_{123} = 6$. By including a localizing force with stabilization energy $E_{loc}/2$, we allow for the possibility of such a delocalized to localized crossover (Figure 4b). Further, the $S = {}^7/_2$ state stabilized is just the one found experimentally $|S\ S^*\ S_{12}\rangle = |^7/_2\ 6\ 4\rangle$. This is not difficult to explain from the fundamental ideas presented earlier. The larger the difference between the Fe^{3+}–Fe^{2+} and the Fe^{2+}–Fe^{2+} Heisenberg interaction (particularly when the former is antiferromagnetic and the latter is ferromagnetic), the more favored is a state where all Fe^{3+}–Fe^{2+} spin pairs are aligned antiparallel and all Fe^{2+}–Fe^{2+} pairs parallel (that is, S^* is maximized). Further the localization energy allows for the selection of a unique Fe^{3+} site. These energy terms must counteract the delocalization energy (B-term E_{res}), which favors a delocalized state with both S^* and S_{12} small; the $S = {}^7/_2$ state with greatest delocalization energy is $|^7/_2\ 1\ 1\rangle$, which has nearly as much delocalization energy as $|^1/_2\ 2\ 4\rangle$. In Figure 4b, we plot the state energy diagram for $f_{loc} = 5$ and $B/J = 6$. This magnitude of localization is sufficient to shift the spin-state crossing point to about $\alpha = -0.25$ instead of -0.5, which is nearer the expected α value predicted by our quantitative calculations.

In Figure 4c, we show the lowest lying states for each total spin at $f_{loc} = 0$ and $B/J = 3$. Clearly, the crossing points between states of different spin are shifted to more positive α compared to $B/J = 6$, as are the crossovers among the different $S = {}^1/_2$ and among the different $S = {}^3/_2$ states. These crossing points will prove to be important when we consider the behavior of the more complicated model in the companion paper. For our present purposes, we note that $|^1/_2\ 2\ 4\rangle$ is the most stable state for $\alpha \gtrsim 0.2$ and that for smaller α there is rapid crossover to other spin states.

In Figure 5, we show how the predicted valence localization $c_A{}^2$ of the four states $|S\ S^*\ S_{12}\rangle = |^1/_2\ 2\ 4\rangle$, $|^3/_2\ 2\ 4\rangle$, $|^5/_2\ 2\ 4\rangle$, and $|^7/_2\ 6\ 4\rangle$ varies with increasing f_{loc} at $B/J = 6$. The following Figure 6 shows how the lower and upper energy bounds of these four states vary as f_{loc} is increased from 0 to 10 for an α range between -0.5 and 1.0. In all cases the lower bound corresponds to α_{min} and the upper bound to α_{max}. Figure 6 provides a good general map of the overall behavior of these spin states. We can consider the upper and lower bounds as defining a tube of possible energy values for the given spin state. As α goes through its range, the energy goes from the lower to the upper bound. Therefore, we know that since $S = {}^7/_2$ completely overlaps $S = {}^1/_2$ (and $S = {}^7/_2$ completely overlaps $S = {}^3/_2$ and ${}^5/_2$ as well), the $S = {}^7/_2$ state will cross below $S = {}^1/_2$ somewhere in the specified α range. Further $S = {}^7/_2$ is preferentially stabilized as f_{loc} increases so that the crossover moves toward more positive α. For spin states that exhibit partial overlap of the tubes such as $S = {}^1/_2$ and $S = {}^3/_2$, such a state crossing may or may not occur. A detailed examination shows that $|^3/_2\ 2\ 4\rangle$ does not cross $|^1/_2\ 2\ 4\rangle$, since both the Heisenberg and the resonance terms are less stable for this ${}^3/_2$ state. As shown in Figure 4b $|^3/_2\ 4\ 4\rangle$ crosses $|^1/_2\ 2\ 4\rangle$ at negative α but $|^7/_2\ 6\ 4\rangle$ descends much more rapidly.

The general theme clearly portrayed in Figures 4–6 is the competition between resonance and localizing forces and similarly of a competition between a large inequality in J_2, J_1 (small or negative α) favoring states with high total S versus states dominated by strong resonance interactions usually (but not always) having low total S. In fact, due to the Heisenberg terms, small or negative α values favor states with large values of S^*, which in turn are most easily achieved when S is large. Clearly, the detailed spin quantum numbers are important, both for substate spin (S^* and S_{12}) as well as total spin. In Figure 7, we show the normalized resonance energy (f_{res}) for all states with $S = {}^1/_2$, ${}^3/_2$, ${}^5/_2$, and ${}^7/_2$. Only the energies at integer quantized values of S_{12} are physically meaningful. This resonance energy behaves as expected for $\langle S_{34} + {}^1/_2\rangle$. For $S = {}^1/_2$ and ${}^3/_2$ the highest resonance stabilization is attained for S_{12} maximal, $S_{12} = 4$ for each curve (i.e. for each value of $|S\ S^*\rangle$). Further, S^* takes on an intermediate value for maximal stabilization. As indicated previously, the state $|^1/_2\ 2\ 4\rangle$ has the maximal resonance stabilization of all states; among the $S = {}^3/_2$ states, $|^3/_2\ 2\ 4\rangle$ has the greatest resonance stabilization. For $S = {}^5/_2$ and ${}^7/_2$, the pattern is basically different. The resonance stabilization does not always increase with increasing S_{12} for given $|S\ S^*\rangle$. Thus, while $|^5/_2\ 2\ 4\rangle$ shows the largest stabilization among $S = {}^5/_2$ states, $|^7/_2\ 1\ 1\rangle$ has the largest among the $S = {}^7/_2$ states. The relative stability of $|^7/_2\ 6\ 4\rangle$ over the other states at small negative α is a clear example of the Heisenberg terms outcompeting the resonance term, since the resonance energy has a quite low value for this level. Further, the localizing forces favor $|^7/_2\ 6\ 4\rangle$ even more and effectively convert this state to a localized state with a unique Fe^{3+} site and a 3:1 equivalence pattern. Where the localization is incomplete, the equivalence pattern is reduced to 2:1:1, reflecting a two Fe^{2+} pair and a partially localized Fe^{3+}–Fe^{2+} mixed-valence pair. The hyperfine properties of this and other important spin states will be addressed in the next section.

VI. Hyperfine and EPR Properties

The observed effective hyperfine parameters A_i for the various Fe centers are related to the corresponding intrinsic site hyperfine

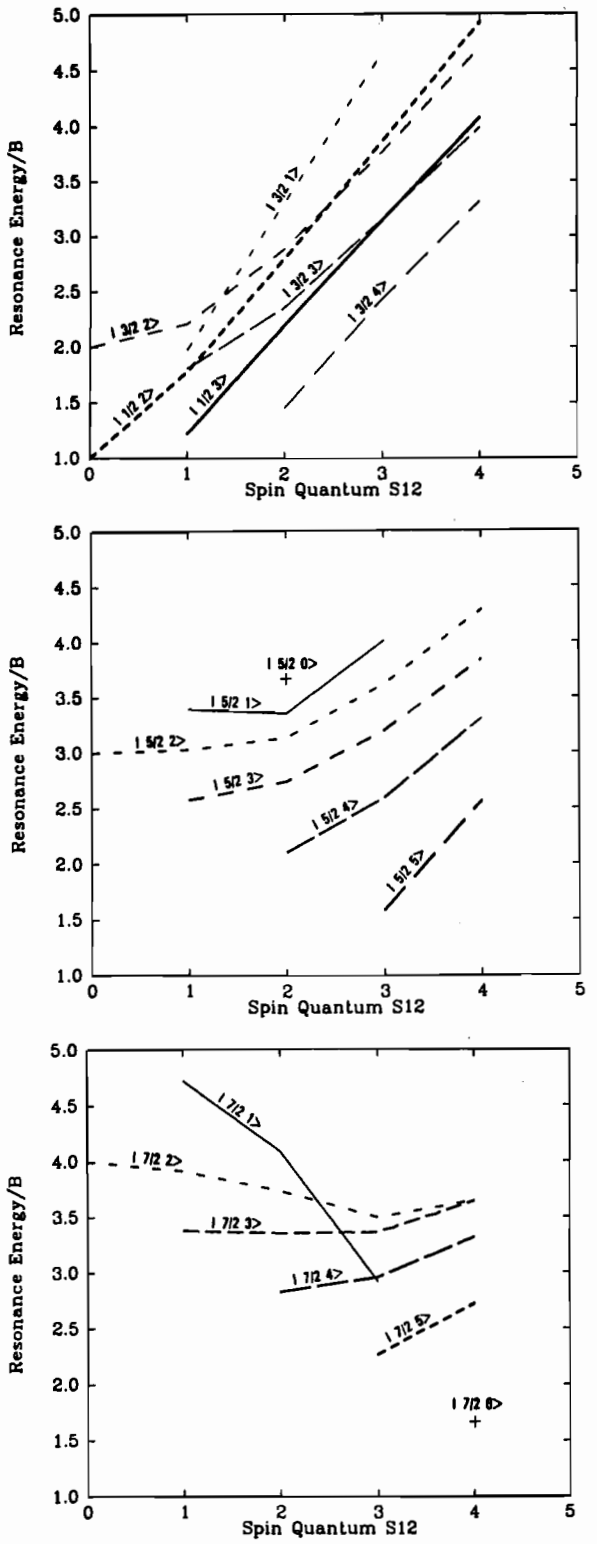

Figure 7. Normalized stabilization energies of all states with $S = {}^1/_2$ to ${}^7/_2$ and eigenvectors $|S\ S^*\rangle$ shown as a function of the spin quantum number S_{12} (only integer values of S_{12} allowed): (a, top) $S = {}^1/_2, {}^3/_2$; (b, middle) $S = {}^5/_2$; (c, bottom) $S = {}^7/_2$.

parameters a_i by application of the Wigner–Eckart theorem for vector operators:[14]

$$A_i = a_i \frac{\langle S_{iz} \rangle}{\langle S_z \rangle} = K_i a_i \tag{16}$$

There is insufficient experimental information to properly treat the full anisotropic A tensor at each site, particularly in the context of the present phenomenological approach. We therefore analyze the data taking a_i to be isotropic for convenience and fixing the values of $a(Fe^{2+}) = -22$ MHz and $a(Fe^{3+}) = -20$ MHz as is typical for Fe–S systems.[9] (We note that the proportional relationship between intrinsic and effective hyperfine parameters should hold for each principal axis direction separately on each site i with the same constants K_i as given in eq 16.[14d]) Correspondingly g_{eff} is given by

$$g_{eff} = \sum_i K_i g_i \tag{17}$$

This equation for g is most useful for $S = {}^1/_2$ states, since for $S > {}^1/_2$, the effect of zero-field splitting (ZFS) on the observed EPR transitions must be taken into account, giving highly anisotropic g values, which are different for each Kramers doublet derived from sublevels of the total spin state. There is good evidence, for example from the existence of spin-"admixed" states in reduced 4Fe-4S clusters, that spin–orbit coupling derived largely from the Fe^{2+} sites will be very important in certain cases, affecting both effective g and A values. (Very often, the effect of ZFS on A values for $S \geq {}^1/_2$ is to strongly emphasize the A tensor values in certain directions in space over others for a particular Kramers doublet.[14e]) Overall, however, a reasonable phenomenological treatment covering a number of important situations is possible based solely on the Wigner–Eckart theorem. Further this approach is a valuable first step in treating the larger problem including ZFS effects.

Again, we express a general state as a linear combination of $c_A|A\rangle + c_B|B\rangle$, where $|A\rangle = |S\ S_A^*\ S_{12}\rangle$ and $|B\rangle = |S\ S_B^*\ S_{12}\rangle$, evaluating the effective site A_i values for states $|A\rangle$ and $|B\rangle$ individually and weighting the result by c_A^2 and c_B^2. Since the properties of $|A\rangle$ and $|B\rangle$ can be determined by precisely analogous methods, it is sufficient to examine the properties of state $|A\rangle$ for the different Fe sites. The site spins are $S_1 = S_2 = S_3 = 2$ and $S_4 = {}^5/_2$. For this spin-coupling pattern, there is nothing to distinguish ferrous sites 1 and 2 in state $|A\rangle$, but site 3 may be different even though it is also high-spin ferrous.

For the ferric site

$$K_4 = \frac{\langle S_{4z} \rangle}{\langle S_z \rangle} = \frac{\langle \vec{S} \cdot \vec{S}_4 \rangle}{S(S+1)} \tag{18}$$

according to the Wigner–Eckart theorem for vector operators. From simple spin-coupling algebra

$$\langle \vec{S} \cdot \vec{S}_4 \rangle = [S(S+1) + S_4(S_4+1) - S_{123}(S_{123}+1)]/2 \tag{19}$$

so that for the ferric site S_4

$$\frac{\langle S_{4z} \rangle}{\langle S_z \rangle} = \frac{[S(S+1) + S_4(S_4+1) - S_{123}(S_{123}+1)]}{2S(S+1)} \tag{20}$$

For one site of the ferrous pair S_1

$$\frac{\langle S_{1z} \rangle}{\langle S_z \rangle} = \frac{\langle S_{1z} \rangle \langle S_{12z} \rangle \langle S_{123z} \rangle}{\langle S_{12z} \rangle \langle S_{123z} \rangle \langle S_z \rangle} \tag{21}$$

In general, if $\vec{S}_Q + \vec{S}_R = \vec{S}_{QR}$ and S_Q, S_R, and S_{QR} are good quantum numbers, then

$$\frac{\langle S_{Qz} \rangle}{\langle S_{QRz} \rangle} = \frac{\langle \vec{S}_{QR} \cdot \vec{S}_Q \rangle}{S_{QR}(S_{QR}+1)} \tag{22}$$

and

$$\vec{S}_{QR} \cdot \vec{S}_Q = \frac{[S_{QR}(S_{QR}+1) + S_Q(S_Q+1) - S_R(S_R+1)]}{2} \tag{23}$$

This relation holds whether Q and R refer to simple indices or to multiple indices. (Further, only S_{QR} and S_Q have to be good quantum numbers for eq 22 to hold; S_R does not have to be. In this situation, the last term of eq 23 is modified by replacing $S_R(S_R+1)$ by $\langle \vec{S}_R \cdot \vec{S}_R \rangle$; that is, by taking an expectation value over $\vec{S}_R \cdot \vec{S}_R$ for the spin eigenstate that results from the full matrix diagonalization. This relationship will prove to be very valuable when the more complex nonlinear model is developed for energies and

Table IV. Hyperfine A_{av} and EPR g_{av} Values for $S = {}^1/_2$ States of $[Fe_4S_4]^+$ Clusters[a]

state or complex	$A(Fe^{3+}$–$Fe^{2+})$, MHz	$A(Fe^{2+}$–$Fe^{2+})$, MHz	g_{av}
	Theory		
$\|{}^1/_2\ 3\ 4\rangle$	+19.1	−31.8	2.14
$\|{}^1/_2\ 2\ 4\rangle$	−33.1	+24.4	1.94
	Experiment		
Av2[b]	−29.7	+15.7	1.96
B st Fd[c]	−30.3	+16.0	1.96
$Fe_4S_4(SR)_4^{3-}$[d]	−31.8	+15.1	1.96

[a] Parameters in the calculations: $\Delta g(Fe^{2+}) = 0.05$, $a(Fe^{2+}) = -22$ MHz, and $a(Fe^{3+}) = -20$ MHz. [b] Av2 protein in ethylene glycol solution.[4] [c] *B. stearothermophilus* Fd.[4,5] [d] $Fe_4S_4(S\text{-}p\text{-}C_6H_4Br)_4^{3-}$.[1]

properties in the companion paper.) By application of eqs 22 and 23 to eq 21

$$K_1 = \frac{\langle S_{1z}\rangle}{\langle S_z\rangle} = K_{1a}K_{1b}K_{1c} \tag{24}$$

where

$$K_{1a} = \frac{[S_{12}(S_{12}+1) + S_1(S_1+1) - S_2(S_2+1)]}{2S_{12}(S_{12}+1)}$$

$$K_{1b} = \frac{[S_{123}(S_{123}+1) + S_{12}(S_{12}+1) - S_3(S_3+1)]}{2S_{123}(S_{123}+1)}$$

$$K_{1c} = \frac{[S(S+1) + S_{123}(S_{123}+1) - S_4(S_4+1)]}{2S(S+1)}$$

For our spin Hamiltonian, there is complete symmetry between sites 1 and 2, so $K_1 = K_2$.

The evaluation of the spin-dependent parameter K_3 for the third ferrous site requires subtler considerations. First of all, using the Wigner–Eckart theorem as in eqs 18 and 21, we have

$$K_i = \frac{\langle S_{iz}\rangle}{\langle S_z\rangle} = \frac{\langle \vec{S}\cdot\vec{S}_i\rangle}{S(S+1)} \tag{25}$$

which applies for site $i = 3$ and, indeed, for all sites. However, when we attempt to use the equation analogous to eq 19, we find that S_{124} is not a good quantum number for state $|A\rangle$. Instead, we can use the following simple theorem

$$\sum_{i=1,4} K_i = \sum_{i=1,4} \frac{\langle S_{iz}\rangle}{\langle S_z\rangle} = \sum_{i=1,4} \frac{\langle \vec{S}\cdot\vec{S}_i\rangle}{S(S+1)} = 1 \tag{26}$$

which is evident since the total spin vector is the sum of the site spin vectors. Therefore

$$K_3 = 1 - K_1 - K_2 - K_4 = 1 - 2K_2 - K_4 \tag{27}$$

Using the equations above, we have calculated effective hyperfine A values for the four sites and the corresponding g_{av} value for different states. In Tables IV–VII, we present results for important low-lying spin states with $S = {}^1/_2, {}^3/_2, {}^5/_2$, and ${}^7/_2$ and compare these with experimental results for a variety of reduced 4Fe-4S states. We assume the following intrinsic site values: $a(Fe^{2+}) = -22$ MHz and $a(Fe^{3+}) = -20$ MHz and $g(Fe^{2+}) = g_0 + \Delta g$ and $g(Fe^{3+}) = g_0$ with $\Delta g = 0.05$ and $g_0 = 2.0023$.[8,9] Clearly, in addition to the dependence of properties on the detailed spin state $|S\,S^*\,S_{12}\rangle$, there is a further dependence on the degree of delocalization or localization of the mixed-valence pair, sites 3 and 4.

For $S = {}^1/_2$ and ${}^3/_2$ we have assumed complete delocalization, $f_{loc} = 0$, and for $S = {}^5/_2$ and ${}^7/_2$ we have assumed either complete or partial localization, $f_{loc} > 0$. For $S = {}^1/_2$, the $|{}^1/_2\ 2\ 4\rangle$ state, which is predicted to be the ground state over most of the range of reasonable B and α (for $6 \le B/J_1 \le 8$, $-0.5 \le \alpha \le 1.0$, while for $B/J_1 = 3$, $0.2 \le \alpha \le 1.0$), has effective $A(Fe^{2+}$–$Fe^{3+}) = -33.1$ MHz, $A(Fe^{2+}$–$Fe^{2+}) = +24.4$ MHz, and $g_{av} = 1.94$ in reasonable agreement with experimental A values and g_{av} for a variety of systems. There is still some discrepancy in A values, typically 3 MHz for the mixed-valence pair and 8 MHz for the ferrous pair.

Table V. Hyperfine A_{av} Values for $S = {}^3/_2$ States of $[Fe_4S_4]^+$ Clusters[a]

state or complex	$A(Fe^{3+}$–$Fe^{2+})$, MHz	$A(Fe^{2+}$–$Fe^{2+})$, MHz
	Theory	
$\|{}^3/_2\ 4\ 4\rangle$	+6.7	−18.7
$\|{}^3/_2\ 1\ 3\rangle$	+8.8	−18.4
$\|{}^3/_2\ 3\ 4\rangle$	+0.2	−11.1
$\|{}^3/_2\ 2\ 4\rangle$	−7.7	−2.4
	Experiment	
Av2/urea[b]	−7.8	−4.1
$Fe_4S_4(SR)_4$[c]	−8.9	−8.9

[a] Parameters in the calculations: $\Delta g(Fe^{2+}) = 0.05$, $a(Fe^{2+}) = -22$ MHz, and $a(Fe^{3+}) = -20$ MHz. [b] Av2 protein in urea solution.[4] [c] $Fe_4S_4(SR)_4^{3-}$, where R = C_6H_{11}.[1]

For $S = {}^3/_2$, the state $|{}^3/_2\ 2\ 4\rangle$ achieves a quite reasonable fit in predicted A values to experimental values observed for Av2 and for a synthetic analogue studied by Carney et al.[1] Despite this, the state $|{}^3/_2\ 2\ 4\rangle$ cannot be considered as proper solution at the present level of theory, since the $S = {}^3/_2$ state that approaches the lowest $S = {}^1/_2$ state is $|{}^3/_2\ 4\ 4\rangle$, as depicted in Figure 4a. Further in the context of the linear model, when $|{}^3/_2\ 2\ 4\rangle$ is below $|{}^3/_2\ 4\ 4\rangle$, it still lies above $|{}^1/_2\ 2\ 4\rangle$. At small or negative α, $|{}^3/_2\ 4\ 4\rangle$ descends rapidly, but this has unsatisfactory hyperfine A values compared with experiment. Certain $S = {}^7/_2$ and $S = {}^5/_2$ states descend even more rapidly than $|{}^3/_2\ 4\ 4\rangle$ at low or negative α, and these are of interest with respect to observed states possessing localized (distinguishable) sites and large S. The situation is greatly improved when the more complete nonlinear model is used.

In Table VII, the hyperfine properties of localized or partially localized states predicted by our linear model are compared with the experimental $S = {}^7/_2$ state of reduced Se-substituted Cp ferredoxin. The fit of either the fully localized or partially localized, $f_{loc} = 5$, state is very good. At $B/J_1 = 6$ and $f_{loc} = 5$ and taking $J_1 = 50$ cm^{-1} approximately, we obtain $E_{loc}/2 = 15J = 2$ kcal/mol, which is of the order of a reasonable site stabilization energy from the protein environment. The simultaneous coexistence of $S = {}^1/_2$, ${}^3/_2$, and ${}^7/_2$ states in reduced Se Cp Fd should be closely related to the predicted crossing point in parameter space depicted in Figure 4a–c. It is likely that the $S = {}^7/_2$ state is to some extent self-trapped. A stabilizing force $f_{loc} = 5$ produces over 90% localization of $|{}^7/_2\ 6\ 4\rangle$ but about 62% localization of $|{}^1/_2\ 2\ 4\rangle$. This would be sufficient, however, to distinguish the two sites of the mixed-valence pair of $|{}^1/_2\ 2\ 4\rangle$ contrary to experiment. The localization energy, therefore, probably arises from the interaction of the protein environment and the $S = {}^7/_2$ state of the cluster and is likely much smaller for $S = {}^1/_2$ and ${}^3/_2$. For example, a dipole-induced dipole interaction between the protein and the cluster would reinforce the stabilization energy of a localized $S = {}^7/_2$ state over that of a more delocalized $S = {}^1/_2$ or ${}^3/_2$ state.

In Table VI, the predicted hyperfine values of some low-lying $S = {}^5/_2$ states are compared with the observed hyperfine values for sites in oxidized P clusters. While the overall fit of the $|{}^5/_2\ 2\ 4\rangle$ hyperfine to experiment is not too bad, there are strong arguments against this being a proper oxidized P cluster ground state. First of all, within the present Hamiltonian, $|{}^5/_2\ 5\ 4\rangle$ is lower in energy over much of the relevant range of α; this state has properties rather like $|{}^7/_2\ 6\ 4\rangle$ and therefore is a poor fit to the hyperfine parameters of oxidized P clusters. Further, the only way $|{}^5/_2\ 2\ 4\rangle$ would give a good fit to the 2:1:1 ($2Fe^{2+}$–Fe^{2+}–Fe^{3+}) site equivalence observed in the hyperfine spectrum is if the mixed-valence Fe^{2+}–Fe^{3+} pair were well localized. From Figure 5, this would require a large localization energy. For sensible parameter values, $|{}^7/_2\ 6\ 4\rangle$ or $|{}^5/_2\ 5\ 4\rangle$ should be lower in energy at small or negative α and $|{}^1/_2\ 2\ 4\rangle$ at larger α. For the oxidized

Table VI. Hyperfine A_{av} Values for $S = {}^5/_2$ State of Oxidized P Cluster $[Fe_4S_4]^+$ [a]

state or signal	$A(2Fe_a^{2+})$, MHz	$A(Fe_b^{2+})$, MHz	$A(Fe_b^{3+})$, MHz
	Theory		
$\|{}^5/_2\ 5\ 4\rangle$	−13.8	−10.0	+14.3
$\|{}^5/_2\ 2\ 4\rangle$	−6.3	+5.0	−13.1
	Experiment		
signal 1	−15.8		
signal 2	−12.1		
signal 5	−14.1		
signal 6	−13.0		
signal 7		+11.0	
signal 8		+12.2	
signal 3			−13.4
signal 4			−8.3
av	−13.8	+11.6	−10.9

[a] Parameters in the calculations: $\Delta g(Fe^{2+}) = 0.05$, $a(Fe^{2+}) = -22$ MHz, and $a(Fe^{3+}) = -20$ MHz. [b] Average is taken over two oxidized P clusters. Experimental data are from ref 3a.

Table VII. Hyperfine A_{av} Values for Localized $S = {}^7/_2$ State of $[Fe_4Se_4]^+$ [a]

state or complex	$A(Fe^{2+})$, MHz	$A(Fe^{3+})$, MHz
	Theory	
$\|{}^7/_2\ 6\ 4\rangle$ [b]	−11.4 (3)	+11.1 (1)
$\|{}^7/_2\ 6\ 4\rangle$ [c]	−11.4 (2), −9.5 (1)	+9.2 (1)
	Experiment	
Se Cp Fd [d]	−10.4 (3)	+8.1 (1)

[a] Parameters in the calculations: $\Delta g(Fe^{2+}) = 0.05$, $a(Fe^{2+}) = -22$ MHz, and $a(Fe^{3+}) = -20$ MHz. [b] The number of equivalent sites is given in parentheses; hyperfine A values for totally localized state. [c] Hyperfine A values for partial localization with parameters $f_{loc} = 5$, $B/J = 6$, and $E_{loc}/2 = 15J$ so that the localization coefficients are $c_A^2 = 0.916$ and $c_B^2 = 0.084$. [d] Reference 2a.

P clusters, a more complicated spin Hamiltonian is evidently required to describe the hyperfine properties and magnetic properties of the system. In fact, the evidence for the oxidized P clusters being reduced 4Fe–4S clusters is not conclusive at present.

VII. Conclusions and Further Questions

From the preceding analysis of energies and properties, both the successes and difficulties of the current model are clear. In contrast to the Heisenberg model, the current model provides a convincing display of the change in site equivalence pattern from 2:2 to 3:1 in response to a localizing perturbation. Sensible g_{av} and hyperfine A values are predicted for the $S = {}^1/_2$ state $|{}^1/_2\ 2\ 4\rangle$, which should constitute the system ground state over a wide range of parameters. The $S = {}^1/_2$ and ${}^7/_2$ coexistence observed in reduced Se ferredoxin corresponds to a crossing point at $-0.5 \leq \alpha \leq 0.0$ in the presence of a physically reasonable localizing force that preferentially traps the mixed-valence sites for $S = {}^7/_2$ and leaves $S = {}^1/_2$ much more delocalized. The hyperfine properties of the $S = {}^7/_2$ localized state are in good agreement with experiment; this state appears as a clear consequence of a large inequality in ferrous versus mixed-valence J parameters plus the effects of an external localizing force. The current model provides a deeper understanding of the empirical spin-coupling model proposed by Auric, Gaillard, and co-workers for the $S = {}^7/_2$ state of Se Cp Fd,[2a] strongly supporting the validity of their model. Near the $S = {}^1/_2$ and ${}^7/_2$ crossing point, there are low-lying excited states nearby in energy having spin $S = {}^3/_2$ and ${}^5/_2$; a nearly degenerate $S = {}^3/_2$ state is observed in reduced Se ferredoxin. The existence of many synthetic analogues with spin-admixed ground states is consistent with the idea that reduced ferredoxins often have parameter values in close proximity to such a crossing point. Quantitative theoretical calculations predict $\alpha = -0.2$ and $B/J_1 = 6$ in related systems with the Fe in similar oxidation states, which is close to the crossing point in the phenomenological description; further, these quantitative calculations give $J(Fe^{2+}\text{–}Fe^{3+}) = 70$ cm^{-1} and $J(Fe^{2+}\text{–}Fe^{2+}) = -15$ cm^{-1} approximately. The mixed-valence Heisenberg interaction parameter J is therefore fairly small (antiferromagnetic), and the ferrous J parameter is smaller and ferromagnetic (or possibly AF and small in some cases). The extreme variability in spin states then becomes quite plausible with a change of 20–30 cm^{-1} in either J parameter (particularly, J_2), leading to major changes in the spin ground state and different spin states easily approaching one another to within 10 cm^{-1}, facilitating strong effects of spin–orbit coupling on the states. The small Heisenberg coupling constants for the reduced 4Fe ferredoxins are in contrast to the much larger AF Heisenberg parameters predicted for high-potential $[Fe_4S_4]^{3+}$ proteins and their synthetic analogues shown in Table III and ref 8. This difference is the major factor determining an $S = {}^1/_2$ ground state for high potential clusters and allowing a wide variety of spin ground states for the reduced clusters.

The important unresolved problems are also clearer after testing out the present linear model. There are systems such as the unusual cluster in [Fe] hydrogenases, which display EPR spectra unlike those of typical reduced ferredoxins; for *Desulfovibrio vulgaris* hydrogenase, two different rhombic EPR signals can be observed with average g values of 1.95 and 2.05 (maximum g values at 2.06 and 2.10, respectively).[18a] There is a correspondingly large change in the A values found from Mossbauer hyperfine studies[19] in this cluster. At present, the best evidence from the electrochemical, Mossbauer, and EPR work of Huynh's group supports the conclusion that this unusual cluster in *D. vulgaris* hydrogenase is a reduced 4Fe–4S cluster.[19] (We note that ENDOR and EPR investigations of Cp hydrogenase I show an EPR g_{av} value of 2.05 with small Fe hyperfine splittings ($|A| = 9.5$, 16 MHz),[18b] but the composition of this is uncertain; it probably contains a 6Fe–xS cluster.[20] It is quite evident that the present linear model cannot represent the variability of the signals in *D. vulgaris* hydrogenase since g_{av} for $|{}^1/_2\ 2\ 4\rangle$ is about 1.94, while for $|{}^1/_2\ 3\ 4\rangle$ $g_{av} = 2.14$. The hyperfine A values for these two states are both large but with opposite relative signs. To obtain a reasonable range and type of variability, we would need to have some type of combination of these basis states. We can readily demonstrate that such states arise from considering all possible resonance interactions over one pair of sites utilizing these basis states. Further, for $S = {}^3/_2$, the hyperfine values for the lowest lying state in the vicinity of the curve crossings are two large and have different signs in contrast to the experimental spectrum; we present a better treatment of $S = {}^3/_2$ states in the following paper.

Finally, there are some problems that are essentially unresolved in present. First, the unusual hyperfine of the oxidized P clusters is entirely unexplained; the ground state here is probably $S = {}^5/_2$ or ${}^7/_2$,[3] but none of our models are convincing with respect to these properties. Second, the occurrence of strongly spin-admixed clusters[1] shows that there are strong spin–orbit effects (ZFS effects) such that total spin is not a good quantum number in these cases. It may be the case that such effects are important in understanding the oxidized P clusters, but this is not known. In any event, the methods necessary to treat this problem are beyond the scope of the present work. There is also the question of the importance of interlayer resonance delocalization to the energies and properties of reduced 4Fe–4S clusters. This is still an unsolved problem, although there are indications from $[ZnFe_3S_4]^+$ and $[Fe_4S_4]^{3+,2+}$ calculations that such effects should be rather small.

In the following companion paper, utilizing a single resonance delocalized pair, we will introduce a more general model that is nonlinear in α. This model directly results from applying the

(18) (a) Patil, D. S.; Moura, J. J. G.; He, S. H.; Teixeira, M.; Prickil, B. C.; DerVartanian, D. V.; Peck, H. D., Jr.; LeGall, J.; Huynh, B. H. *J. Biol. Chem.* **1988**, *263*, 18732. (b) Telser, J.; Benecky, M. J.; Adams, M. W. W.; Mortenson, L. E.; Hoffman, B. M. *J. Biol. Chem.* **1986**, *261*, 13536.
(19) Huynh, B. H. Personal communication.
(20) Munck, E. Personal communication.

present resonance Hamiltonian to a complete set of basis states and yields further significant improvements in the description of $S = {}^1/_2, {}^3/_2$, and ${}^7/_2$ states as well as spin crossover phenomena.

Acknowledgment. I thank D. A. Case, P. Yip, E. Munck, J. Girerd, V. Papaefthymiou, J. Gaillard, and B. H. Huynh for valuable discussions and the National Institutes of Health (Grant GM39914) for financial support. I also thank J. P. Desclaux for providing the Racah coefficient and matrix diagonalization routines.

Contribution from the Department of Molecular Biology, MB1, Research Institute of Scripps Clinic, La Jolla, California 92037

Exchange Coupling and Resonance Delocalization in Reduced $[Fe_4S_4]^+$ and $[Fe_4Se_4]^+$ Clusters. 2. A Generalized Nonlinear Model for Spin-State Energies and EPR and Hyperfine Properties

Louis Noodleman

Received April 16, 1990

I develop a generalized nonlinear model for the spin states of reduced $[Fe_4S_4]^+$ and $[Fe_4Se_4]^+$ clusters. This model is an extension of that described in the previous paper and allows the internal electron transfer within the mixed-valence pair to couple together a larger set of basis states. The consequences of this model for the energies and properties of various states with spin $S = {}^1/_2$, ${}^3/_2$, and ${}^7/_2$ are explored. For a range of parameters similar to that used previously, we find that the lowest $S = {}^3/_2$ state appears in much closer proximity to the lowest $S = {}^1/_2$ state over an extended range of the $\alpha = J_2/J_1$ parameter compared with the preceding linear model. Such a near proximity of $S = {}^1/_2$ and ${}^3/_2$ is consistent with the statistical mixtures of these states often found in reduced $[Fe_4S_4]^+$ and $[Fe_4Se_4]^+$ clusters. The observed crossing points among $S = {}^1/_2$, ${}^3/_2$, and ${}^7/_2$ are consistent with the observed coexistence of these three states in $[Fe_4Se_4]^+$ at low temperatures. In addition to providing reasonable predictions for average g and A values for $S = {}^1/_2$ states in typical reduced 4Fe ferredoxins, the model shows how the large variation in average g values, 1.97 and 2.05, for the two different rhombic states observed in *Desulfovibrio vulgaris* hydrogenase can arise from a modest variation in $0.2 \leq \alpha \leq 0.5$ at low B/J, $3 \leq B/J \leq 2.5$. The predicted variability in average g values is a consequence of the nonlinear model; the linear model cannot give a satisfactory account of this variability. We obtain a good theoretical prediction of the small negative hyperfine constants observed by Mossbauer spectroscopy on all Fe sites in the lowest $S = {}^3/_2$ state for various clusters. The nonlinear theory gives a far better prediction of hyperfine constants for $S = {}^3/_2$ than the linear theory. The predicted theoretical A_{av} values for the Fe^{2+} and Fe^{3+} sites of the $S = {}^7/_2$ state in Se-substituted Cp ferredoxin are well represented by the nonlinear model; at least partial localization of the mixed-valence pair by extrinsic forces is indicated. The Zeeman parameter g_0' determined by EPR spectroscopy is also calculated with reasonable accuracy by the model.

I. Introduction

In the preceding paper (P 1),[1] I developed a basic model for spin-state energies and spin-dependent properties (g and A values) for reduced $[Fe_4S_4]^+$ and $[Fe_4Se_4]^+$ clusters. In this paper, I generalize this model in the most direct way possible. No new parameters are introduced, but significant improvements in the physical realism of the model are obtained by simply allowing all possible iinteractions of basis states with the same Hamiltonian as in P 1. For the same range of parameters previously used, the lowest $S = {}^3/_2$ state appears in much closer energetic proximity to the lowest $S = {}^1/_2$ state, as might be inferred empirically from the prevalence of statistical mixtures of $S = {}^1/_2$ and $S = {}^3/_2$ states in reduced $[Fe_4S_4]^+$ and $[Fe_4Se_4]^+$ clusters at very low temperatures; quantum admixtures of $S = {}^1/_2$ and ${}^3/_2$ have also been inferred from analysis of EPR and magnetization data in some cases.[2] We also obtain a good description of the small hyperfine coupling displayed by the lowest $S = {}^3/_2$ state when this is the lowest spin state overall or when there is coexistence of $S = {}^1/_2$, ${}^3/_2$, and ${}^7/_2$ low-lying states.[3] The more general model displays variability in predicted g and A values for each spin state as the location in parameter space is altered. This variability provides a reasonable explanation for the observed differences in g values of the two different rhombic states seen by EPR spectroscopy for an unusual cluster in *Desulfovibrio vulgaris* hydrogenase.[4] The hyperfine properties of the $S = {}^7/_2$ state in Se-substituted *Clostridium pasteurianum* ferredoxin are well described by the nonlinear model.

While the present nonlinear model is more accurate quantitatively than the linear model and better justified on fundamental grounds, there is also considerable value in the simpler linear model. The linear model involves only the diagonalization of 2 × 2 matrices; hence all energies are obtained as roots of quadratic equations. By contrast, the nonlinear model requires in general diagonalization of larger matrices (maximum size 10 × 10 in some cases); the resulting behavior of the energy roots is more complicated and difficult to understand. For qualitative understanding, it is probably best to begin with the states and energies of the linear model and to think of the additional off-diagonal terms of the nonlinear model as a perturbation on these. This perturbative mixing of states becomes large when a pair of linear states with the same S and S_{12} quantum numbers approach one another (i.e., for linear states differing only in S^*), and there is consequently a noncrossing rule for these states. These eigenstates will cross in the linear model but not in the nonlinear model. Further, there is a qualitative change in the nature of the lowest eigenstate as it passes through the region of near crossing in the nonlinear model, since there is strong mixing of basis states in this region. Conversely, if all interacting states with the same S and S_{12} values

(1) Noodleman, L. *Inorg. Chem.*, preceding paper in this issue.
(2) Carney, M. J.; Papaefthymiou, G. C.; Spartalian, K.; Frankel, R. B.; Holm, R. H. *J. Am. Chem. Soc.* **1988**, *110*, 6084.
(3) (a) Auric, P.; Gaillard, J.; Meyer, J.; Moulis, J. M. *Biochem. J.* **1987**, *242*, 525. (b) Gaillard, J.; Moulis, J. M.; Auric, P.; Meyer, J. *Biochemistry* **1986**, *25*, 464. (c) Moulis, J. M.; Auric, P.; Gaillard, J.; Meyer, J. *J. Biol. Chem.* **1984**, *259*, 11396.
(4) (a) Patil, D. S.; Moura, J. J. G.; He, S. H.; Teixeira, M.; Prickil, B. C.; DerVartanian, D. V.; Peck, H. D., Jr.; LeGall, J.; Huynh, B. H. *J. Biol. Chem.* **1988**, *263*, 18732. (b) Telser, J.; Benecky, M. J.; Adams, M. W. W.; Mortenson, L. E.; Hoffman, B. M. *J. Biol. Chem.* **1986**, *261*, 13536.

0020-1669/91/1330-0256$02.50/0